Atomic Structure of PDE4: Insights into Phosphodiesterase Mechanism and Specificity

Robert X. Xu,[1] Anne M. Hassell,[1] Dana Vanderwall,[1] Millard H. Lambert,[1] William D. Holmes,[2] Michael A. Luther,[2] Warren J. Rocque,[2] Michael V. Milburn,[1] Yingdong Zhao,[3]* Hengming Ke,[3]† Robert T. Nolte[1]†

Cyclic nucleotides are second messengers that are essential in vision, muscle contraction, neurotransmission, exocytosis, cell growth, and differentiation. These molecules are degraded by a family of enzymes known as phosphodiesterases, which serve a critical function by regulating the intracellular concentration of cyclic nucleotides. We have determined the three-dimensional structure of the catalytic domain of phosphodiesterase 4B2B to 1.77 angstrom resolution. The active site has been identified and contains a cluster of two metal atoms. The structure suggests the mechanism of action and basis for specificity and will provide a framework for structure-assisted drug design for members of the phosphodiesterase family.

Cyclic nucleotides are intracellular second messengers that play a key role in many physiological processes. The levels of these nucleotides are tightly regulated at the point of synthesis by receptor-linked enzymes (such as adenylyl or guanylyl cyclase) and at the point of degradation by a family of enzymes known as phosphodiesterases (PDEs). The PDEs constitute a large, divergent family whose members catalyze the hydrolysis of adenosine 3′,5′-monophosphate (cAMP) and guanosine 3′,5′-monophosphate (cGMP), resulting in the formation of the 5′-nucleotide metabolites (AMP and GMP). Ten PDE gene families have been identified, and more than 50 mRNA splicing isoforms have been detected in various human tissues [reviewed in (*1*–*5*)] (*6*). These isoforms are differentially expressed and regulated in different cell types, and they appear to modulate the location, substrate selectivity, kinetics, and response to activators or inhibitors of the enzyme (*7*–*9*). PDEs are clinical targets for a range of biological disorders such as retinal degeneration, congestive heart failure, depression, asthma, erectile dysfunction, and inflammation (*10, 11*). Knowledge of the structure of a PDE will allow for the rational design of therapeutics to treat many of these disorders.

[1]Department of Structural Chemistry, [2]Department of Molecular Sciences, Glaxo Wellcome Research and Development, Research Triangle Park, NC 27709, USA. [3]Department of Biochemistry and Biophysics, University of North Carolina at Chapel Hill, Chapel Hill, NC 27599, USA.

*Present address: Molecular Statistics and Bioinformatics Section, National Cancer Institute, Bethesda, MD 20892, USA.

†To whom correspondence should be addressed.

The structure of the catalytic domain (residues 152 to 528) of human phosphodiesterase 4B2B (PDE4B2B) was determined by multiwavelength anomalous dispersion in combination with multiple isomorphic replacement (Tables 1 and 2) (*12*). The catalytic domain of PDE folds into a novel compact structure composed of 17 α helices, which form three subdomains (Fig. 1). The first subdomain forms a bundle of four α helices (H3, H5, H6, and H7), with two short interconnecting α helices (H2 and H4). The residues of H0 and H1 are poorly conserved across the PDE family and may not be an essential part of the catalytic domain (*13*). The second subdomain is formed by two short α helices (H8 and H9) that sit perpendicular to a pair of long antiparallel α helices (H10 and H11). The third subdomain is composed of five α helices (H12 to H16) and an extended loop that forms a β hairpin between H12 and H13. Helix 15 (H15a/H15b) is kinked by partially conserved Pro^{453} and is probably a continuous helix in the absence of proline. In one of the two molecules in the asymmetric unit, residues 496 to 508 form an additional helix (H17), which packs against a neighboring molecule in the crystal. We believe that the position of this helix is an artifact of crystallization and is not a relevant dimer contact.

A deep pocket in the center of the COOH-terminal subdomain extends to the junction of the three subdomains. Of the 21 residues absolutely conserved across all 10 PDE families, 20 lie near this pocket and 12 lie within it (Fig. 2) (*13*). The pocket has a volume of 440 $Å^3$ and is the only pocket large enough to accommodate a molecule of the cAMP substrate (232 $Å^3$) or AMP product (256 $Å^3$). The pocket is lined with conserved hydrophobic and negatively charged residues. At the bottom of the pocket are several metal atoms, which bind to residues that are completely conserved in all PDE family members.

One of these metal atoms (ME1) coordinates residues in H6 in subdomain 1, the loop between H7 and H8 (linking subdomains 1 and 2), and H13 in subdomain 3. ME1 may stabilize the structure by acting as a linchpin that locks the three subdomains of the protein together. It may also play a catalytic role because of its proximity to the active site. ME1 has a high occupancy (as indicated by the intensity of the peaks in electron density maps) and is located deepest in the pocket (Fig. 3). It was present despite the presence of chelators and the absence of additional exogenous divalent metal ions during the purification or crystallization of the protein. ME1 interacts with the N_ε atoms of His^{238} (2.0 Å) and His^{274} (2.1 Å) and the O_δ atoms of Asp^{275} (2.3 Å) and Asp^{392} (2.2 Å) in a trigonal bipyramid configuration where the Asp residues occupy the axial positions (Fig. 3). The remaining equatorial position is occupied by a solvent atom (1.9 Å), which also acts as a bridging ligand to a second metal ion. Although the identity of the metal ions cannot be absolutely determined from our structure, the observed geometry of the metal coordinating ligands, the anomalous x-ray diffraction behavior, the existing biochemical evidence (*14*–*17*), and the known high affinity of PDE4 for zinc (*18*) all suggest that ME1 is a Zn^{2+} ion.

The second metal ion (ME2) varied in occupancy between crystals when no additional metal ions were added to the solution. However, it was always highly occupied when exogenous metals (Mn, Mg, or Zn) were added to the protein. ME2 makes only one direct interaction with the enzyme to the

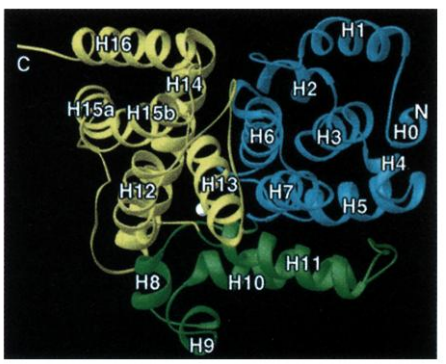

Fig. 1. Ribbon diagram of the secondary structure of the catalytic domain (residues 152 to 489) of PDE4B2B. ME1 is shown as a silver sphere (ME2 is behind H13 in this orientation). The NH_2-terminal subdomain of the molecule (residues 152 to 274) is colored cyan, the middle subdomain green (residues 275 to 347), and the COOH-terminal subdomain is colored yellow (residues 348 to 489).

Table 1. X-ray data and phasing statistics. Data sets for $SmCl_3$ and $GdCl_3$ were collected on beamline 17ID at the Advanced Photon Source in Argonne National Laboratory (APS); all others were collected on beamline X12C at the National Sychrotron Light Source in Brookhaven National Laboratory (NSLS). All data were processed with the HKL package (*36*).

Data set	Wavelength (Å)	Resolution (Å)	Completeness (%)	Number of reflections	R_{sym}*	R_{iso}†	Phasing power iso/ano‡
$ErCl_{3(remote)}$	1.432	2.50	100	31,783	0.061	0.182	0/2.02
$ErCl_{3(peak)}$	1.482	2.50	99	31,551	0.103	0.181	1.58/2.65
$ErCl_{3(inflection)}$	1.483	2.50	99	31,578	0.107	0.178	2.18/2.30
$SmCl_3$	1.000	2.50	100	31,033	0.138	0.198	0.84/0.88
$GdCl_3$	1.000	2.40	98	34,336	0.165	0.206	1.08/0.85
K_2PtCl_4	1.080	2.80	100	22,755	0.109	0.221	1.23/0.38
Native	1.080	1.77	100	88,528	0.058	—	1.08/0

*$R_{sym} = \Sigma_{hkl}|I - \langle I\rangle|/\Sigma I$, where I is the observed intensity and $\langle I\rangle$ is the average intensity from observations of symmetry-related reflections. †$R_{iso} = \Sigma_{hkl}||F_{PH}| - |F_P||/\Sigma(|F_{PH}| + |F_P|)$, where F_P and F_{PH} are the structure factor amplitudes from the native and heavy atom derivative, respectively. ‡Phasing power of isomorphous (iso) difference and anomalous (ano) difference measurements.

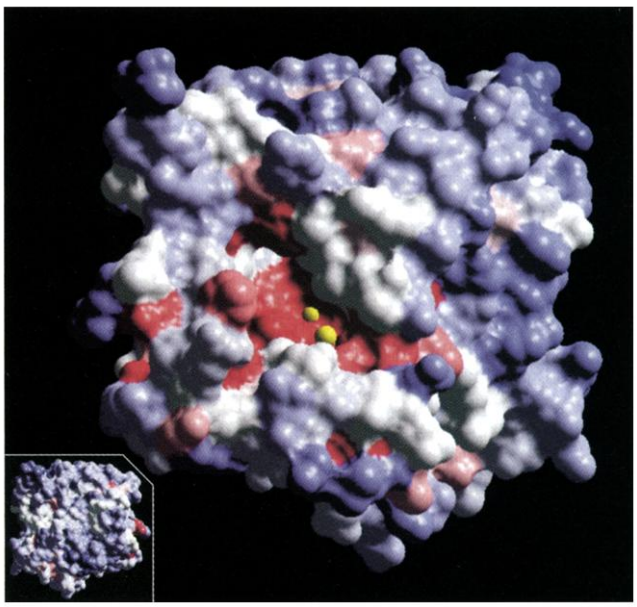

Fig. 2. Surface representation of the PDE4 molecule. The orientation of this view is an 80° counterclockwise rotation around the vertical axis of that shown in Fig. 1. The surface colors denote the level of sequence conservation across the 10 PDE families. Completely conserved residues are shown in red, partially conserved residues in white, and highly variable residues in blue. ME1 and ME2 are represented as yellow spheres. A view of the opposite side of the molecule is shown in the inset at the lower left.

second O_δ of Asp^{275} (2.4 Å). It further interacts with the water molecule (2.4 Å) that binds to the first metal ion. Four additional water molecules complete the distorted octahedral geometry of the second metal site. These water molecules in turn form hydrogen bonds with residues His^{278}, Glu^{304}, His^{307}, and Ser^{345} of the enzyme. The preferred in vivo ion cannot be determined from this study. Others have shown that many ions are capable of supporting enzymatic activity (*19, 20*); however, it is likely that either Mn^{2+} or Mg^{2+} is the relevant physiological ion (*21*). ME1 and ME2 coordinate several of the residues found in the two highly conserved PDE sequence motifs His-Asn-X-X-His (residues 234 to 238) and His-Asp-X-X-His (residues 274 to 278), each of which was previously considered to form a separate metal binding site (*22*).

The two metal ions are ~3.9 Å apart and constitute a binuclear motif similar to that found in other enzymes that catalyze the hydrolysis or formation of amide or phosphate bonds. The motif in PDE is particularly similar to that found in the active site of 3′,5′-exonuclease of DNA polymerase I Klenow fragment, which contains Zn^{2+} and Mg^{2+} ions with similar coordination spheres (*23*). Little else about the active site of PDE4 resembles these enzymes.

A model of cAMP docked in the PDE4B2B active site (Fig. 4) shows that a water molecule coordinated to one or both metal ions could act as the nucleophile in the hydrolysis reaction. The metal ions would also serve to stabilize the transition state. The strictly conserved His^{234} is positioned to accomplish the protonation of the O3′ leaving group. The position of His^{234} is maintained by a hydrogen bond between its N_δ and a carboxylate oxygen of Glu^{413}, which is itself

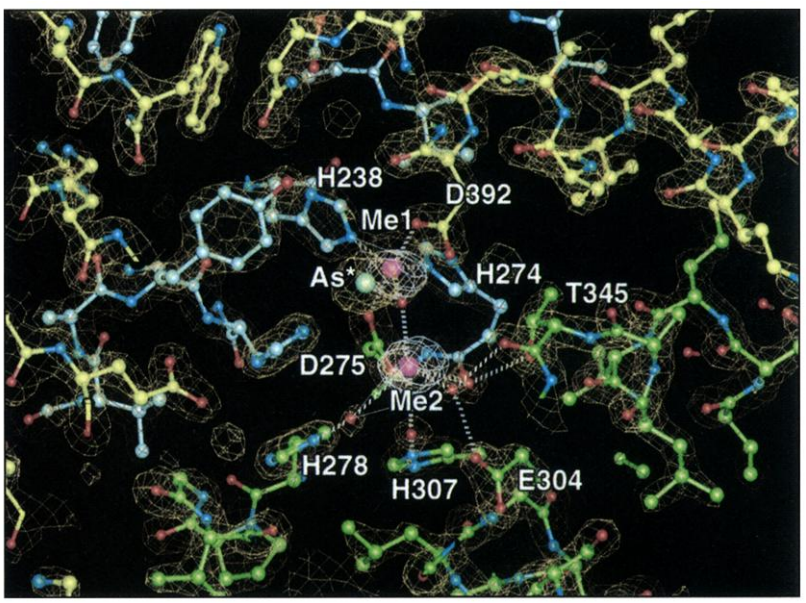

Fig. 3. Overview of the active site. A $2F_{obs} - F_{calc}$ electron density map of the metal binding site calculated from 18 to 1.77 Å native data is shown in brown at a level of 2.5σ. An anomalous difference map calculated from 20 to 3.3 Å using refined phases and data from an Er-soaked crystal collected at λ = 1.48 Å is shown in gray at a level of 5σ. ME1 and ME2 are shown in magenta, water molecules are red, and the protein carbon atoms are colored as in Fig. 1. Metal ion interactions are shown in white. Several observations indicate that a third metal ion visible in the electron density is a crystallization artifact arising from an opportunistic arsenate ion (As*) present in the crystallization buffer. This ion shows variable occupancy and makes only three water-mediated contacts with the protein. Anomalous difference density at the site of the third metal ion (shown in cyan) was observed in data collected at λ = 1.0 Å but not in data collected at λ = 1.4 Å, which is consistent with an arsenate ion. The position of the arsenate ion, 2.6 Å above the water that bridges the two metal atoms, suggests a possible binding site for phosphate, or a phosphate-containing species in the active site.

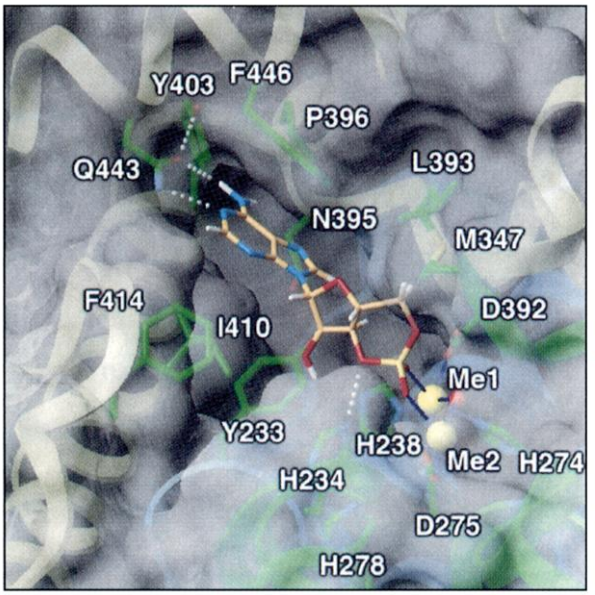

Fig. 4. Model of cAMP bound to PDE4. A molecular docking procedure was used to fit cAMP into the proposed active site (*34*). The preferred model is shown in which cAMP adopts the anti conformation with the adenine base inserted into a lipophilic pocket formed by Leu^{393}, Pro^{396}, Ile^{410}, Phe^{414}, and Phe^{446}. The cyclic phosphate group binds to ME1 and ME2, replacing the observed arsenate ion shown in Fig. 3. The 1-N and 6-NH_2 groups form hydrogen bonds with the side chain of Gln^{443}, while the 7-N position forms a more distorted hydrogen bond with Asn^{395}. The ribose ring binds loosely against Met^{347} and Leu^{393}, with a hydrogen bond between His^{234} and the O3′ oxygen, but with no obvious interaction to the O2′, O4′, and O5′ atoms. Consistent with our model, an experimental synthetic cAMP analog study found that PDE4 makes important interactions with the 1-N, 6-NH_2, and 7-N positions, but not with the 2′-OH (*35*).

stabilized by hydrogen bonds between the other side-chain oxygen and two backbone amides (Tyr^{233} and His^{234}). The ring of His^{234} is stacked against the ring of His^{278} and with the edge of the aromatic ring of Tyr^{233}. These stacking and hydrogen bond interactions to three other conserved residues further stabilize the position of His^{234} and probably alter the pK_a of the N_ε so it more closely matches that of the O3′ phosphate ester. The enzyme appears to have committed four amino acids to donate a proton, which speaks to the importance of this protonation step in the evolution of this enzyme to catalyze cAMP hydrolysis.

The proposed binding mode of cAMP (Fig. 4) also offers insight into cAMP and cGMP specificity within the PDE superfamily. Compared with adenine, guanine has a 1-NH, a 2-NH_2, and a 6-CO group on the purine base. The hydrogen-bonding character at the 1- and 6- positions is thus essentially reversed. Gln^{443}, which "reads" the 1- and 6- position groups in the anti conformation model, is conserved in all 10 PDE gene families. However, this glutamine could accommodate the 1- and 6-position groups in cGMP by rotating its amide group by 180°. The reversible hydrogen-bonding character of glutamine should thus permit hydrolysis of both cAMP and cGMP, as occurs in dual-specificity PDEs. In PDE4, Tyr^{403} forms a hydrogen bond with Gln^{443} and provides additional steric constraints that may be responsible for the cAMP specificity. Residues proximal to Gln^{443} in the other PDEs may likewise influence its orientation and optimize the shape of the pocket to favor binding of specific nucleotides.

The PDE4 structure further clarifies the functions of many other residues that were characterized in the PDE family. For example, mutations of residues in rat PDE3 corresponding to PDE4 His^{307} and Thr^{345} completely diminished the enzyme activity (*24*). His^{307} and Thr^{345} are in the cAMP binding pocket and serve a critical function by forming water-mediated interactions to the second metal ion, positioning it for efficient catalysis. Other studies have implicated several residues on helix 14 in cAMP-cGMP specificity (*25*). One of these residues (Thr^{407}) makes direct contacts with the nucleotide base in our docked substrate model, whereas the other residue (Tyr^{403}) appears to play a key role in orienting Gln^{443}.

Previous studies have shown that rolipram, an efficient inhibitor of PDE4, is a competitive inhibitor (*26*) and binds with a stoichiometry of 1:1 within the catalytic domain (*27*). Well-characterized mutations that affect rolipram binding (*28*) are primarily located in the binding pocket, and many of these residues are predicted to be in contact with the cAMP substrate in our model. It is likely that many of the known PDE inhibitors bind within the active-site pocket. The PDE4B2B crystal structure, as a representative of this therapeutically important class of enzymes, will assist the drug discovery process by providing binding and specificity information based on the crystal structure.

Table 2. Refinement statistics.

Resolution range	18.0 to 1.77 Å
Reflections in working set	82,005
Reflections in test set	2541
R_{cryst}*	20.20%
R_{free}†	22.7%
Number of non-hydrogen protein atoms	5554
Number of solvent molecules	751
RMS deviation from ideal	
Bond lengths	0.0050 Å
Bond angles	1.13°
B factor	
Average protein	26.5
Average solvent	38.5
RMS bonded atoms	0.554

*$R_{cryst} = \Sigma_{hkl}||F_{obs}| - |F_{calc}||/\Sigma|F_{obs}|$, where F_{obs} and F_{calc} are the observed and calculated structure factor amplitudes, respectively, for the *hkl* reflections. †R_{free} is calculated for a set of reflections that were not included in atomic refinement (*33*). Both R_{cryst} and R_{free} are calculated with no σ cutoff.

References and Notes

1. M. Conti and S. L. C. Jin, *Prog. Nucleic Acid Res. Mol. Biol.* **63**, 1 (1999).
2. M. D. Houslay, M. Sullivan, G. B. Bolger, *Adv. Pharmacol.* **44**, 225 (1998).
3. V. C. Manganiello, T. Murata, M. Taira, P. Belfrage, E. Degerman, *Arch. Biochem. Biophys.* **322**, 1 (1995).
4. T. J. Torphy, *Asthma* **2**, 1755 (1997).
5. A. Z. Zhao, C. Yan, W. K. Sonnenburg, J. A. Beavo, *Adv. Second Messenger Phosphoprotein Res.* **31**, 237 (1997).
6. K. Loughney *et al.*, *Gene* **234**, 109 (1999).
7. M. D. Houslay and G. Milligan, *Trends Biochem. Sci.* **22**, 217 (1997).
8. J. A. Beavo, *Physiol. Rev.* **75**, 725 (1995).
9. R. E. Weishaar, M. H. Cain, J. A. Bristol, *J. Med. Chem.* **28**, 537 (1985).
10. M. Conti, S. L. C. Jin, L. Monaco, D. R. Repaske, J. V. Swinnen, *Endocr. Rev.* **12**, 218 (1991).
11. M. M. Teixeira, R. W. Gristwood, N. Cooper, P. G. Hellewell, *Trends Pharmacol. Sci.* **18**, 164 (1997).
12. PDE4B2B protein was prepared as described (*29*). Diffraction-quality crystals were obtained using vapor diffusion by combining a 1:1 ratio of protein solution with a polyethylene glycol (PEG-3000) precipitant. X-ray diffraction data from native and derivatized crystals were collected at −170°C. The crystals diffract in space group $C222_1$, with unit cell dimensions of a = 104.5 Å, b = 159.6 Å, c = 109.0 Å. The location of the initial heavy atom sites was determined by the Patterson method and anomalous difference Fourier maps using the CCP4 program suite (*30*). Final experimental phases to 2.4 Å were calculated using SHARP (*31*), which yielded an overall figure of merit of 0.63. The resulting phases were improved and extended to 1.8 Å by density modification and noncrystallographic averaging with the CCP4 program DM. Alternating cycles of model building with the program O (*32*) and refinement using experimental phase constraints with the program CNS (*33*) were used to determine the final structure. Continuous electron density is observed from the NH_2-terminal residue 152 to residue 489 for both molecules in the asymmetric unit. No density was observed for residues 490 to 495 and residues 509 to 528.
13. For sequence alignment and secondary structure assignment of representative members from the 10 PDE gene families, see *Science* Online (www.sciencemag.org/feature/data/1050158.shl).
14. M. D. Houslay, *Semin. Cell Dev. Biol.* **9**, 161 (1998).
15. J. Londesborough, *Biochem. J.* **225**, 143 (1985).
16. R. J. Marchmont and M. D. Houslay, *Nature* **286**, 904 (1980).
17. R. J. Marchmont, S. R. Ayad, M. D. Houslay, *Biochem. J.* **195**, 645 (1981).
18. S. H. Francis, J. L. Colbran, L. M. McAllister-Lucas, J. D. Corbin, *J. Biol. Chem.* **269**, 22477 (1994).
19. M. D. Percival, B. Yeh, J.-P. Falgueyret, *Biochem. Biophys. Res. Commun.* **241**, 175 (1997).
20. S. M. Callahan, W. Cornell Neal, P. V. Dunlap, *J. Biol. Chem.* **270**, 17627 (1995).

21. I. Wilkinson, P. Engels, M. D. Houslay, *Pharmacol. Rev. Commun.* **9**, 215 (1997).
22. G. A. Omburo, S. Jacobitz, T. J. Torphy, R. W. Colman, *Cell. Signalling* **10**, 491 (1998).
23. L. S. Beese and T. A. Steitz, *EMBO J.* **10**, 25 (1991).
24. S. L. C. Jin, J. V. Swinnen, M. Conti, *J. Biol. Chem.* **267**, 18929 (1992).
25. I. V. Turko, S. H. Francis, J. D. Corbin, *J. Biol. Chem.* **273**, 6460 (1998).
26. G. P. Livi *et al.*, *Mol. Cell. Biol.* **10**, 2678 (1990).
27. W. J. Rocque *et al.*, *Biochemistry* **36**, 14250 (1997).
28. J. M. Atienza, D. Susanto, C. Huang, A. S. McCarty, J. Colicelli, *J. Biol. Chem.* **274**, 4839 (1999).
29. W. J. Rocque *et al.*, *Protein Expr. Purif.* **9**, 191 (1997).
30. Collaborative Computational Project No. 4, *Acta Crystallogr.* **D50**, 760 (1994).
31. E. De La Fortelle and G. Bricogne, *Methods Enzymol.* **276**, 472 (1997).
32. T. A. Jones, J. Y. Zou, S. W. Cowan, M. Kjeldgaard, *Acta Crystallogr.* **A47**, 110 (1991).
33. A. T. Brünger *et al.*, *Acta Crystallogr.* **D54**, 905 (1998).
34. Candidate syn and anti binding modes of cAMP and cGMP were generated in and around the metal site with Ligand Fit (Cerius2) and also by graphical manipulation. The most plausible binding modes were refined with CHARMm (MSI) or MVP (Glaxo Wellcome) and ranked according to their LUDI (MSI) or MVP scores. ME1 and ME2 were modeled as Zn^{2+} and Mg^{2+}, respectively, and the low-occupancy arsenate ion was omitted.
35. E. Butt *et al.*, *Mol. Pharmacol.* **47**, 340 (1995).
36. Z. Otwinowski and W. Minor, *Methods Enzymol.* **276**, 307 (1997).
37. Coordinates of the PDE4B2B catalytic domain may be obtained from the Protein Data Bank, accession code 1F0J. We thank R. Sweet (NSLS beamline X12C), J. Chrzas (APS beamline 17-ID), Y. Xia and R. Gampe for technical assistance, E. Xu for useful discussions, and P. Jeffs for encouragement and support. Supported by NIH grant AI33072 (H.K.).

7 March 2000; accepted 21 April 2000

Signaling Specificity by Frizzled Receptors in *Drosophila*

Michael Boutros,* Jozsef Mihaly, Tewis Bouwmeester, Marek Mlodzik†

Wnt-Frizzled (Fz) signaling pathways play recurring important roles during the development and homeostasis of vertebrates and invertebrates. Fz receptors can signal through β-catenin–dependent and –independent pathways. In *Drosophila*, Fz and Fz2 are redundant receptors for Wg. In addition, Fz conveys signals through a distinct pathway to organize planar polarization of epithelial structures. We demonstrate that the cytoplasmic sequences of Fz2 and Fz preferentially activate the β-catenin and planar polarity cascade, respectively. Both receptors activate either pathway, but with different efficiencies. Intrinsic differences in signaling efficiency in closely related receptors might be a general mechanism for generating signaling specificity in vivo.

Pattern formation in multicellular organisms relies on specific inductive signaling events. Many evolutionarily conserved signaling pathways are used at multiple times during development to induce tissue- and cell type–specific responses (*1*). Despite the importance of context-dependent signaling specificity, the underlying mechanisms have remained elusive.

Frizzled (Fz) proteins act as receptors for Wnt ligands. Most Wnt-Fz signal transduction pathways involve the posttranslational stabilization of the intracellular protein β-catenin (β-cat/Arm) (*2*, *3*). However, some Fz receptors can also signal through pathways independent of the Wnt–β-cat (Wg-Arm) cascade (*4*–*8*). Both pathways use Dishevelled (Dsh) as a transduction component, raising the intriguing question of how two structurally related receptors signal through a common protein into distinct effector pathways. In *Drosophila*, Fz and Fz2 are redundant receptors for Wg, activating the Wg-Arm cascade (*9*–*13*). Nevertheless, functional differences between Fz and Fz2 in Wg-Arm signaling remain. Fz2 has a higher affinity for Wg than Fz (*12*, *14*), and removal of either Fz or Fz2 has subtle, but different, effects on the patterning of the embryonic nervous system (*9*). Moreover, only Fz is specifically required for epithelial planar polarity by signaling through a Wg-Arm–independent pathway (*4*, *6*, *7*).

Fz overexpression during *Drosophila* eye development (*15*) causes a gain-of-function (GOF) planar polarity phenotype (*4*, *16*). Overexpression of Fz2 in the developing wing activates Wg-Arm targets (*14*, *16*). To compare the functional equivalence of Fz and Fz2 (we will refer to Fz as Fz1) for activating either the planar polarity or Wg-Arm pathways, Fz1 and Fz2 were expressed with tissue-specific enhancers (*17*) in imaginal discs during *Drosophila* development (*18*). Whereas Fz1 overexpression in eye (Fig. 1A) (*4*, *16*) and wing discs (*19*) resulted in planar polarity phenotypes, Fz2 expression led to planar polarity defects with only very low penetrance (<1%) (Fig. 1B). Conversely, overexpression of Fz2 in wing imaginal discs led to formation of ectopic bristles [a *wg* GOF phenotype (*14*, *16*, *19*)], whereas Fz1 overexpression did not affect bristle formation (*16*, *19*). Thus, Fz receptors have distinct signaling abilities in imaginal discs, despite their redundant role for Wg-Arm signaling in loss-of-function (LOF) analysis (*9*–*13*).

To assess Wnt–β-cat signaling in a quantifiable in vitro assay, we injected both receptors into *Xenopus* embryos and analyzed Wnt target induction in animal cap explants (*20*–*23*). In this heterologous assay, Fz2 induced strong activation of the Wnt–β-cat targets Xnr-3 and Siamois (Sia), whereas Fz1 induced a much weaker response (Fig. 1C). Thus, taken together with the imaginal disc phenotypes, Fz2 is a strong activator of Wnt–β-cat signaling, and Fz1 is a potent activator of the planar polarity pathway. However, both receptors retain a low intrinsic potential to cross-activate either pathway.

Differential Dsh localization may determine Fz signaling specificity, whereby Fz1, but not Fz2, can induce recruitment of Dsh to the membrane in *Xenopus* (*6*). At normalized protein levels for Fz1 and Fz2, however, we did not observe differences in their ability to recruit Dsh (Fig. 1D). Titration experiments with Fz1 and Fz2 RNA concentrations showed very similar threshold levels for either receptor in Dsh membrane localization (*24*). Thus, differential Dsh recruitment is unlikely to be the mechanism by which specificity between these Fz receptors is generated.

Fz receptors are serpentine transmembrane proteins composed of an extracellular ligand-sequestering domain (CRD), a seven-pass transmembrane segment, and a COOH-terminal cytosolic tail (*25*, *26*) (Fig. 2). To determine which domains in Fz1 and Fz2 are required for directing signaling into either pathway, we constructed chimeric and truncated receptors (Fig. 2) (*27*). These chimeric proteins were tested for their signaling potential in *Drosophila* imaginal disc development in wings and nota (with *apGal4*) (*28*), eyes (*15*), and legs (*29*) for their ability to induce either GOF Wg-Arm signaling (Figs. 2 and 3) or planar polarity phenotypes (Figs. 2 to 4).

Both Fz1-2 and Fz1-1-2 chimeric proteins activated a Wg-Arm target (Ac) in the wing imaginal disc (Fig. 3B), induced ectopic marginal bristles (Figs. 2 and 3, G to I), and showed *wg*-associated effects in the leg (*29*). However, they had no significant effect on planar polarity signaling in the eye, the wing, or the notum (Figs. 2, 3, G to I, and 4, C and F). Thus, the Wg-Arm signaling outcome corresponded with the presence of the Fz2 cytoplasmic tail. In contrast, GOF planar polarity phenotypes were observed with chimeric Fz2-1 receptors in the wing (Fig. 3K), the notum (*28*), and the eye

European Molecular Biology Laboratory, Developmental Biology Programme, Meyerhofstrasse 1, 69117 Heidelberg, Germany.

*Present address: Harvard Medical School, Department of Genetics, 200 Longwood Avenue, Boston, MA 02115, USA.

†To whom correspondence should be addressed. E-mail: mlodzik@embl-heidelberg.de